

# Soft Sensor for Bottom-Hole Pressure Estimation in Petroleum Wells Using Long Short-Term Memory and Transfer Learning

Mateus A. Fernandes<sup>a,b,d</sup>, Eduardo Gildin<sup>c</sup>, Marcio A. Sampaio<sup>a</sup>

<sup>a</sup>*University of São Paulo, Brazil*

<sup>b</sup>*Petrobras, Brazil*

<sup>c</sup>*Texas A&M University, USA*

<sup>d</sup>*Corresponding Author, matfern@usp.br*

---

## Abstract

Monitoring bottom-hole variables in petroleum wells is essential for production optimization, safety, and emissions reduction. Permanent Downhole Gauges (PDGs) provide real-time pressure data but face reliability and cost issues. We propose a machine learning-based soft sensor to estimate flowing Bottom-Hole Pressure (BHP) using wellhead and topside measurements. A Long Short-Term Memory (LSTM) model is introduced and compared with Multi-Layer Perceptron (MLP) and Ridge Regression. We also pioneer Transfer Learning for adapting models across operational environments. Tested on real offshore datasets from Brazil's Pre-salt basin, the methodology achieved Mean Absolute Percentage Error (MAPE) consistently below 2%, outperforming benchmarks. This work offers a cost-effective, accurate alternative to physical sensors, with broad applicability across diverse reservoir and flow conditions.

*Keywords:* petroleum industry, soft sensors, long short-term memory, transfer learning, neural networks.

---

## 1. Introduction

One of the primary challenges in petroleum engineering is dealing with the lack of direct access to the source of natural resources: the subsurface reservoir rock. Throughout the exploration and production (E&P) life cycle, this challenge is addressed in various ways. For instance, during the exploration

phase, we rely on indirect data acquisition, such as seismic surveys, while in the early development phase, we obtain partial insights through rock samples collected during drilling operations. However, the most enduring source of information throughout the life cycle of wells and reservoirs is their behavior during production. Measurements of pressure, temperature, and production rates over time, although taken sparsely at the well locations, form the foundation for detecting anomalies, early identification of production loss events (e.g., scaling or reservoir damage), understanding reservoir configuration, forecasting future performance, and ultimately guiding actions and projects aimed at optimizing recoverable volumes [1], as well as operational and environmental safety and, ultimately, value addition. The availability of continuous and reliable data for these variables during the productive life of a well is therefore critical for disciplines such as reservoir engineering, well testing, flow assurance, and operations management [2].

In offshore production systems, the most relevant nodes for such measurements are:

- Bottom-hole: where pressures and temperatures are measured by the Permanent Downhole Gauges (PDGs).
- Christmas tree at the wellhead: where the same variables are tracked via temperature and pressure transducers (TPTs).
- Topside of the platform: where we find sensors for pressure and temperature both upstream and downstream of the choke valves (the ones which regulate the flow rate and pressure for each well), as well as flowmeters and monitoring systems for oil, gas, and water rates. A schematic of an offshore production system, highlighting its basic components and the aforementioned analysis nodes is shown in Fig. 1 [3].

The PDGs, positioned at the wellbore's bottomhole and closest to the reservoir, serve as the most critical sensors for reservoir management and production monitoring [4]. While these sensors are widely employed in high-yield offshore wells, the deployment and maintenance expenses for the instruments themselves, along with their accompanying monitoring infrastructure, often render them economically unfeasible in many scenarios. This is particularly evident in mature fields and in cases where low productivity or short well lifespan is anticipated. As a result, in practice, PDGs are installed in only a minority of wells across the industry.

When PDG data is inaccessible, obtaining bottom-hole pressure measurements typically relies on periodic wireline interventions. Those operations require interruptions in production to deploy downhole testing equipment. Even in wells originally equipped with PDGs, data accessibility may be compromised over time due to gauge malfunctions or communication breakdowns with topside monitoring systems [5]. Operating for extended periods in high-pressure, inaccessible downhole environments, these sensors have the highest failure risk, and their replacement demands complex workover operations that are generally economically prohibitive [6].

An alternative for unavailable sensor conditions is virtual metering (soft sensors). This approach can be based upon techniques as machine learning, mathematical relationships, statistical methods, and potential integrations with other tools to monitor process variables when physical measures (hard sensors) cannot be used, including hostile environments, information delays, and others [7].

This work focuses on developing a data-driven soft sensor for flowing bottomhole pressure estimation. Here we emphasize that the proposed applicability is limited to steady-state flow pressure. This pressure is lower than the reservoir's static pressure, resulting in the pressure differential required for fluid flow from the porous medium to the wellbore, as described by Darcy's Law [8].

This alternative is designed to address scenarios where physical downhole gauges are unavailable or to serve as a component of a digital twin system (referring to a virtual representation of equipment or processes) [9]. In such cases, the machine learning-estimated BHP can be continuously compared to the actual measurements, providing a reference value for error detection and anomaly identification.

The following section brings a contextualization, providing an overview of traditional approaches and state-of-the-art methods for this task, and inserting the proposed solution within current technological gaps. Section 3 presents the proposed methodology, systematically explaining each step of model development. Section 4 brings the results and discusses their practical implications, while Section 5 summarizes key conclusions.

## 2. Contextualization and Objectives

In oil production, we deal with a complex case of multiphase flow through pipelines with varying geometries, resulting in diverse flow patterns. This

combination of factors poses significant challenges for modeling, leading the industry to rely primarily on empirical, data-driven, or hybrid solutions. In this section, we detail the problem and highlight some of the most relevant existing solutions, as well as the gap that our work aims to bridge.

### *2.1. Problem Statement*

A fundamental characteristic in oil production is the gas liberation due to depressurization, once the bubble-point pressure is reached. This process initiates with the lighter hydrocarbon fractions of the mixture transitioning from liquid to gas phase [10], occurring either in the reservoir after depletion or during its flow toward the surface. The conditions required for bubble point pressure to be reached vary over time, depending on pressure drops along the flow path, restrictions in well openings such as choke valves, reservoir drainage status, and changes in produced fluid composition, which may also change temporally (concept drift) due to reservoir characteristics or injection breakthrough.

The multiphase flow eventually becomes more complex over time, as water production generally increases coming from injection or aquifer influx [8], resulting in three concomitant phases.

Flow geometry further complicates the system: production typically involves vertical flow in the well tubing, transitions to horizontal flow in seabed-mounted flowlines (in offshore systems), and resumes vertical flow in risers leading to the platform. Deviations such as downward flow sections may occur in configurations like lazy-wave risers, adding further variability to flow patterns [11].

Other influencing factors include well control valve operations—particularly the choke valve, which regulates production by introducing a pressure drop that affects the entire flow system—as well as intelligent completion equipment (used to modify the open reservoir interval for production) and artificial lift methods. For example, gas lift, a common artificial lift technique, reduces the average fluid density by injecting gas into the wellbore, thereby lowering the flowing BHP [12]. This method is illustrated in Fig. 2.

This combination of factors can lead to multiple flow patterns along the wellbore and pipelines, from bottomhole to the surface, often varying over time depending on well conditions. In vertical pipes, common flow regimes include bubble, slug, churn, annular, and wispy, while horizontal flow typically exhibits annular, bubble, stratified, and intermittent patterns. Pipe orientation significantly influences these regimes: vertical flow maintains axial

symmetry, whereas horizontal flow tends toward stratification due to gravitational effects [13].

The interplay of changes in flow patterns, mass transfer between phases, and slippage between phases establishes complex nonlinear relationships in pressure gradients [14], where gravitational, frictional, and accelerational components:

$$\frac{dP}{dL} \Big|_{Total} = \frac{dP}{dL} \Big|_{grav} + \frac{dP}{dL} \Big|_{fric} + \frac{dP}{dL} \Big|_{accel} \quad (1)$$

where  $dP/dL$  are the pressure drops along the lengths of tubing and pipelines, and each component responds differently to changing flow regimes, fluid compositions, and control actions. This represents a challenge for obtaining precise analytical modeling and even for accurate numerical simulations that are valid for a broad range of conditions [13].

## 2.2. Traditional Methods

Traditional multiphase flow modeling relies heavily on empirical correlations derived from experimental data. Some of the more notable works in this area are listed in the next paragraphs, which continue to be widely used in the industry decades after their publication:

Duns and Ros (1963) [15]: developed a correlation for estimating pressure gradients in vertical multiphase flow, based on experimental data covering a broad range of oil–gas mixtures with varying water cuts. The method incorporates flow regime maps to identify flow patterns and estimates pressure drops by accounting for liquid holdup, phase slippage, frictional losses, and acceleration effects. The method remains widely adopted due to its accuracy in high gas fraction scenarios, including production under gas-lift.

Hagedorn and Brown (1965) [16]: also worked with vertical flow, based on full-scale experimental data. Their method assumes steady-state, homogeneous flow and incorporates pressure- and temperature-dependent fluid properties, used in iterative liquid holdup calculations. The authors intended to obtain a more general correlation, and for that relied on dimensionless groups and avoided segregation for different flow patterns. This generalization allows accurate predictions across a wide range of tubing sizes, flow conditions, and fluid compositions. However, its accuracy diminishes in deviated or horizontal wells due to increased flow regime complexity.

Beggs and Brill (1973) [14]: were pioneers in developing a correlation capable of handling inclined pipes at any angle. Their method accounts for

different flow regimes (segregated, intermittent, and distributed) and calculates pressure gradients using holdup and friction factor adjustments. It is widely used in the petroleum industry due to its versatility and accuracy in modeling multiphase flow in production tubing and flowlines

These correlations are present even in the foundations of many commercial simulation tools, due to their computational efficiency and proven performance in conventional scenarios.

Despite their widespread use, these correlations tend to be limited by their calibration for particular conditions, which reduces their accuracy when applied to a broader range of production scenarios. As wells and fields evolve over time, changes in flow regimes can lead to reduced reliability, especially as production dynamics shift. Additionally, many empirical models simplify physical phenomena, such as phase slippage or assuming homogeneous fluid, which can lead to inaccuracies under complex conditions [17].

Mechanistic models, while based in flow physics, also face similar challenges while assuming a single flow regime and oversimplifying governing dynamics [18].

As production systems continue to diversify, e.g. high-GOR shale wells or CO<sub>2</sub>-rich flows, the rigidity of these correlations poses a growing challenge for accurate performance prediction and optimization.

The limitations of application ranges also affect simulation software. While these tools are capable of providing more precise estimates for pressure and temperature gradients, performing sensitivity analyses, managing gas lift operations, and calculating flow rates from boundary pressures, they still depend on models that require periodic updates to parameters reflecting current well conditions, such as inflow performance relationships (IPR) [17].

### 2.3. Current Research

With the advent of data-driven, artificial intelligence, and deep learning methods, this area of research headed to a new direction. Those methods offer an advantage here by enabling the development of soft sensors even when the relationships between variables are not explicitly known. This characteristic is useful for gaining new insights and exploring novel applications. Developments on analytical and numerical solutions, nonetheless, are still useful for studies of multiphase flow, especially in cases where we must calculate pressure losses in tubing and pipelines [19]. In specific cases, integrating physics-based equations, computational simulations, and machine learning algorithms has demonstrated advantages [20].

The use of data-driven methods for estimating well parameters has gained substantial traction in field operations. As noted by Aguirre et al. [21], these methods are increasingly replacing conventional instrumentation for real-time monitoring and even automated process control. In recent literature, we find a variety of approaches for the problem of estimating BHP under different circumstances, as we exemplify in the next paragraphs.

Zheng et al. [6] addressed the problem by employing knowledge-guided machine learning. They incorporated physics-based loss functions into NN and XGBoost models to enhance accuracy, which proved important as they were dealing with a small dataset, consisting of data from two wells in a gas field at the early stage of development.

Zalavadia et al. [18] developed a hybrid model that, in the first phase, selects the most suitable physics-based correlation for each sample and then refines the estimate using physics-informed machine learning. They used a combination of static (e.g., PVT) and dynamic (e.g., rates and sensor data) inputs, achieving strong results with simple regression methods due to the hybrid approach. Campos et al. [22] estimated flowing BHP using bottom-hole temperature, wellhead pressure, flow rates, depth, and tubing internal diameter as inputs for radial basis function (RBF) neural networks, with weights optimized through particle swarm optimization (PSO). Using a similar set of input variables, Nwanwe and Duru [23] gave preference to a white-box approach, using an adaptive neuro-fuzzy model, which performed significantly better than empirical correlations and mechanistic models. Opoku et al. [24] calculated BHP for an oil well using empirical correlations in the form of a system of linear equations, selected through a Quasi-Monte Carlo method.

The complexity of applying data-driven methods to real-world cases is highlighted by Antonelo et al. [2]. The authors show that, for a simulated model, the reproduction of BHP is possible even using only one input variable, the choke bean size. However, for real, noisy data obtained from wells operating with gas lift and under slug flow, a much more complex framework was required. Nevertheless, they achieved good results using Echo State Networks.

Firouzi and Rathnayake [25] focused on coal seam gas wells, collecting both surface and subsurface data from five wells over observation periods extending to 18 months. They classified these wells into groups based on flow characteristics and added a categorical variable to represent these groups. Their comparative analysis revealed neural networks' superior performance over regression methods, which they linked to the networks' effectiveness in

modeling non-linear relationships.

In their approach to estimating flowing BHP in a tight sand gas condensate field, Al Shehri et al. [26] used wellhead pressure and temperature, depth, fluid specific gravity, chloride content, water cut, and fluid rates as inputs. They emphasized the narrow application range of classical correlations and presented results showing that neural networks could outperform these correlations. They also implemented a LSTM model, although its performance was not the best.

Olamigoke and Onyeali [27] also evaluated different methods for estimating flowing BHP, with LSTM outperforming both Random Forest and Support Vector Regression (SVR) when tested on two wells from the Volve field, following optimization of the input feature combinations.

Sanusi et al. [28] presented an alternative methodology for BHP estimation in wells operating with Electrical Submersible Pump (ESP) systems, employing a hybrid approach combining Response Surface Methodology (RSM) with neural networks. Their model utilized key ESP parameters including intake and discharge pressures, temperatures, current draw, and pump speed as predictive inputs.

Agwu et al. [29] employed multivariate adaptive regression splines (MARS) to estimate BHP, using eight input variables and training the model with 1,001 data points sourced from the literature. They emphasized the model's high accuracy, interpretability, and physical validation, making it well-suited for practical and real-time applications. These authors also conducted an extensive review, presenting a chronological analysis of data-driven methods for BHP estimation. They systematically tabulated the employed methodologies, dataset characteristics, applicability, and associated error margins.

The variety of methods and applications documented in recent literature demonstrates how machine learning is enabling solutions tailored to specific conditions and grounded in available data. We observe, however, that *existing studies have not adequately addressed flowing BHP estimation under conditions of pronounced concept drift and domain shift, characterized by substantial inter-well and temporal variations in production parameters.*

In our previous work [30], we explored the possibilities of a deep learning approach using LSTM, obtaining improvements when compared to simpler neural networks, validating over time for diverse production conditions, and showing suitability for practical, real-time applications.

In this study, we expand the scope by incorporating a significantly broader dataset and a wider range of operational conditions. Notably, we also pioneer

the use of transfer learning to address bottom-hole pressure estimation in oil wells, with the goal of developing a generalized and scalable framework that can be used across multiple oilfields with varying characteristics.

#### *2.4. Objectives and Contributions*

This study aims to develop a methodology for estimating the flowing bottom-hole pressure in oil wells during regular operation, leveraging a data-driven approach based on supervised learning (including deep learning).

To achieve this, we implement and evaluate multiple configurations of Long Short-Term Memory (LSTM) and Multi-Layer Perceptron (MLP) neural networks, as well as regularized linear regression. Using these supervised learning methods, we intend to extract knowledge and “learn” the fluid flow dynamics in well tubing and production flowlines to estimate BHP from surface measurements and wellhead gauge data, without relying on analytical models, empirical equations, or the properties of produced fluids. This selection of methods ranges from widely-used basic techniques to one of the most prominent latest advances in deep learning.

Additionally, we evaluate the benefits of transfer learning for this task, using the models trained with the dataset from an oilfield that has longer history and larger number of wells as a base model to be adapted to another field where the available data for training is limited and the production conditions is different, including the use of artificial lift.

Our motivation is to obtain a virtual meter capable of estimating BHP reliably enough to be used in well and reservoir monitoring actions, including real-time possibilities, being able to be deployed when physical sensors for bottom hole measurements are unavailable. We highlight that the proposed methodology is intended to be widely applicable across different fields and operational scenarios where similar surface measurements exist, particularly in cases where PDGs are impractical due to cost or technical constraints.

The main contributions of this work are:

- Use of time-related data with deep learning for improved pressure estimation.
- Broad operational applicability, validated across diverse reservoir conditions and production scenarios.
- Use of transfer learning, enabling adaptability to new oilfields and changing operational conditions.

- Potential application in practical scenarios as a virtual meter in wells without available PDGs, including real-time monitoring.

### 3. Methodology

This section details the data acquisition process, analyzes key attributes of the dataset, and presents the machine learning framework developed for BHP estimation. Our methodology for addressing this challenge is systematically organized in the workflow diagram provided in Fig. 3.

We implemented the solution in Python, relying on available interfaces with the Plant Information (PI) real-time monitoring system, and the operator company’s production databases.

#### 3.1. Database

We used as a case study data collected over 13 years from two distinct offshore oilfields located in the Brazilian pre-salt basin, including 09 platforms and a total of 60 oil producing wells, with 45 of them in our first oilfield, that for confidentiality reasons we will call Field 1, and the other 15 wells in the so-called Field 2.

An important characteristic of this particular dataset is the diversity of reservoir and fluid conditions across both spatial and temporal domains. This complexity is a consequence of a superposition of factors: (1) regional variations in initial fluid composition due to the reservoir’s expansive dimensions; (2) uneven evolution of drainage progression across different regions of the reservoir; (3) lithological heterogeneities; and (4) recovery strategies used over time, including Water Alternating Gas (WAG) injection. These factors, plus differences in perforation depths, well geometries and flowline lengths, lead to a large variety of flow conditions. Such diversity results in a challenging problem, as we want our machine learning to estimate BHP with good accuracy in this plethora of conditions.

In those fields, as a project assumption all wells have one or more PDGs installed at completion, but we observed that a relevant number of these became unavailable since then. As we stated in our previous work [30], downhole gauge failure is approximately three times more frequent than its counterparts located at the wellhead, due to the harsh operating conditions (high pressures and temperatures) [6] and the longer distances for signal traveling. Also, their replacement is far more complex and expensive.

Variable	Node	Unit
Bottom-hole Pressure (BHP)	Bottom-hole (PDG)	$kgf/cm^2$
Bottom-hole Temperature (BHT)	Bottom-hole (PDG)	$^{\circ}C$
Wellhead Pressure (WHP)	Wellhead (TPT)	$kgf/cm^2$
Wellhead Temperature (WHT)	Wellhead (TPT)	$^{\circ}C$
Choke upstream pressure	Platform	$kgf/cm^2$
Choke upstream temperature	Platform	$^{\circ}C$
Choke valve aperture	Platform	%
Oil production rate	Platform	$m^3/d$
Gas production rate	Platform	$Mm^3/d$
Water production rate	Platform	$m^3/d$
Gas-lift injection rate	Platform	$Mm^3/d$

Table 1: **List of variables used for the supervised learning.**

The variables we assumed as relevant to estimate BHP and that are readily available in the operator company’s databases are shown in Table 1, including node of measurement and units.

Production rates are calculated daily by allocating platform-level totals to individual wells based on their latest production test results, a methodology that introduces inherent uncertainty due to the proration process. All other well parameters, including the BHP itself, are sourced from the PI monitoring system, which provides continuous, high-frequency recordings.

While bottom-hole temperature (BHT) data is available, we deliberately excluded it from our analysis. This decision aligns with our objective to estimate BHP under conditions where PDG signals are absent, as the predominant failure mode [5] involves concurrent loss of both pressure and temperature measurements.

The two oilfields that compose our dataset present distinct characteristics in terms of location, reservoir properties, and production parameters, as we show in Table 2 with a statistical summary of the variables. A comparison of the most relevant variables for both fields is shown in the boxplots in Fig. 4. We observe that, on average, Field 2 has higher pressures, gas-to-oil ratios (GORs), water cuts, and well depths compared to Field 1. Another important difference is that Field 1 shows minimal and almost negligible use of gas lift, while Field 2 has had wells using this method for longer periods. These characteristics provide favorable conditions for the application of a transfer learning framework, as they allow for the exploration of how data

Stats.	Field	Depth PDG (m)	Oil rate ( $m^3/d$ )	Gas rate ( $Mm^3/d$ )	Water rate ( $m^3/d$ )	Choke Open. (%)
mean	1	4804.7	3168.9	832.3	150.3	68.3
mean	2	4879.4	3169.2	1075.9	532.6	48.8
std-dv	1	65.7	1134.6	296	307.5	37.1
std-dv	2	49.8	1483.9	504.4	922.2	40.5
min	1	4547.5	52.6	9.6	0	4
min	2	4782.3	55.6	30.2	0	4
max	1	4921.7	7111.8	2150.2	2776.9	125
max	2	4966.3	10294.3	3284.1	5622.3	103.2
Stats.	Field	Press. Choke in. ( $kgf/cm^2$ )	Temp. Choke in. ( $^{\circ}C$ )	WHP ( $kgf/cm^2$ )	WHT ( $^{\circ}C$ )	BHP ( $kgf/cm^2$ )
mean	1	38.8	28.1	207.3	52.5	404.1
mean	2	58.9	34	264.1	54.8	462.2
std-dv	1	28.9	8.3	40.2	4.2	48.8
std-dv	2	37.6	7	46.3	3.8	45.1
min	1	0	0.1	100	2.6	111.6
min	2	3.1	0.6	100.1	2.5	127.8
max	1	208.4	100	335.9	71.8	521.9
max	2	214.1	82.1	375.3	76.8	540.7

Table 2: **Statistical summary of the dataset.**

from one field can benefit the learning process for another without having to retrain an entire model, and also taking advantage of its ability to generalize across different data distributions.

Our dataset encompasses a wide array of operational conditions and production parameters for both fields, being one of the largest (with more than 100,000 samples) and most comprehensive in the related literature, as we can see when compared to the compilation made by [29]. Those characteristics are particularly important when dealing with deep learning methods that are data-intensive. This dataset offers a solid foundation for validating the methodology and demonstrates its potential for application to other platforms or fields.

### 3.2. Data Conditioning and Feature Engineering

Once the scope of our problem is defined, we start the sequence of steps for data conditioning and feature engineering, fundamental to feed the ML methods with quality data, maximizing their potential.

1) Our first step is loading the datasets using a Python API that integrates with the company's databases for production records and with the Plant Information monitoring system. The latter is capable of providing real-time monitoring of the most relevant sensors in the production system, registering every second—we export as hourly averages to better suit our purpose. Production data is registered with daily periodicity, where official measurement is performed for the total volume of the platform, and a share is attributed to each well based on its most recent production test. These tests are made by directing the production of a single well to a test separator to have its production rates monitored for a determined time [17]. This can be considered a drawback and a possible limitation for the accuracy of our estimators, since alterations in individual well behavior can remain unnoticed until the next test, which can take up to three months.

2) Data cleaning is performed by removing all samples with at least one null or error value, those with production rates or choke aperture equal to zero (to ensure we deal only with flowing BHP), and the ones where the well remained open for less than 2 hours during a day, which could represent transients.

3) We implemented a simple anomaly detector to remove “frozen” sensor data, actuating when the measured values remain erroneously constant for more than 3 days.

4) We aligned all variables to the same time base, calculating daily averages for the sensor data. This resulted in 69,039 total samples from Field 1, and 29,799 from Field 2.

5) We added to the dataset derived variables calculated from production rates, the gas-oil ratio (GOR):

$$GOR = \frac{Q_g}{Q_o} \quad (2)$$

and the Water Cut:

$$W_{cut} = \frac{Q_w}{(Q_o + Q_w)} \quad (3)$$

where  $Q_o$ ,  $Q_g$ , and  $Q_w$  represent oil, gas, and water production rates, respectively. The new variables can be used as an alternative to gas and water rates in our dataset, with lower variability.

6) The next step is dataset partitioning. For Field 1, we separated two different subsets for blind tests: one consisting of the entire history for a group of 09 wells, and the other with the last year of history of all wells, simulating a future application scenario. The remaining data is used for training and validation, segmented for 5-fold cross validation [31]. Fig. 5 illustrates this partitioning.

For Field 2, consisting of only two platforms, we separated data from one of them for testing (07 wells), and also used the last year of all wells as a second test dataset. The remaining data is used for training, considering that despite the limited number of samples, we can benefit from the transfer learning framework using knowledge from Field 1.

7) Outlier removal is based on Inter-Quartile Ranges (IQR) to remove a sample  $i$  if any of its variables  $x_i$  satisfies the conditions for the lower limit:

$$x_i < Q_1 - 1.5 \cdot IQR \quad (4)$$

and higher limit:

$$x_i > Q_3 + 1.5 \cdot IQR \quad (5)$$

where  $Q_1$  and  $Q_3$  are the values for which the Cumulative Distribution Function for  $x$  equals to 25% and 75%, respectively, and  $IQR = Q_3 - Q_1$ . Exceptions are made if deviations slightly larger than the threshold are physically plausible, e.g., oil rates in wells operating temporarily with restrictions. We perform that step separately for our two datasets, given that the fields have different statistical distributions.

8) An analysis of the correlations among the variables can be used to support the selection of the best set of inputs for our regression problem. Using the training/validation dataset for Field 1, we generated the correlation heatmap shown in Fig. 6, consisting of values calculated using Pearson's coefficient [32]:

$$r = \frac{\sum_{i=1}^n (x_i - \bar{x}) \cdot (y_i - \bar{y})}{\sqrt{\sum_{i=1}^n (x_i - \bar{x})^2 \cdot (y_i - \bar{y})^2}} \quad (6)$$

where  $r$  is the correlation coefficient,  $x_i$  and  $y_i$  the samples of two different sets of variables,  $\bar{x}$  and  $\bar{y}$  their respective mean values, and  $n$  the number of

samples.

9) Next, we performed data normalization, evaluating two different approaches: Gaussian normalization using mean and standard deviation, and the *MinMax* normalization limiting the ranges of all variables to the interval  $[0, 1]$ . The latter can avoid extreme value ranges compared to the first approach, but at the same time it can compress relevant values to a narrower range [33]. Normalization parameters are calculated using only training data (separately for the two datasets), preventing information leakage from the validation and test sets. Violin plots showing the distribution of the variables after this step, for the example of Field 1 with *MinMax* normalization, are presented in Fig. 7.

10) Finally, we construct time-dependent input samples for the LSTM model. For this, each sample will carry values for a number of previous time steps, as we exemplify in Fig. 8. There, we have  $n$  input variables and  $p$  previous time steps feeding the LSTM to estimate BHP at a time  $t$ . For the other benchmark methods, not time-related, we consider  $p = 0$  and have as inputs only the variables measured at the current time.

### 3.3. Aspects of the Machine Learning Methods

In this work, we evaluated three machine learning methods to address the proposed task. A concise overview of those methods is provided, with comprehensive implementation details available in the referenced literature. We also bring some considerations about transfer learning and its applications.

1) *Multivariable Linear Regression*: This method serves as our first benchmark due to its simplicity, low computational cost, and interpretability. Linear regression assumes that the outputs can be expressed as a weighted sum of the input features [34]. Model training consists of determining optimal weights that minimize a loss function applied to the training dataset [35].

Variants of linear regression can include regularization terms that act as penalties for the regression coefficients. This approach helps prevent overfitting by reducing the influence of input variables that may capture noise or outliers, promoting models with improved generalizability. Regularization thereby balances predictive accuracy with computational tractability, valuable in scenarios with limited training data or high-dimensional input spaces.

Ridge regression adds a term in the equation of the loss function (that will be minimized in the training phase), as shown below:

$$f_{ridge} = \sum_{i=1}^n [y_i - (w \cdot x_i + b)]^2 + \alpha \cdot \sum_{j=1}^p w_j^2 \quad (7)$$

where  $y$  is the predicted value,  $x$  is the input value,  $w$  and  $b$  the coefficients to be adjusted. The last term, responsible for the regularization, is weighted by a factor  $\alpha$ , which can be tuned to control the penalties of the regression coefficients. Setting  $\alpha = 0$  reduces the equation to the simple linear regression, while large values may exaggeratedly shrink the coefficients [36]. We use the regression based on 7, with  $\alpha$  as a hyperparameter adjusted during the training and validation of the model.

2) *Neural Networks*: As our second benchmark model, we selected a NN using the traditional Multilayer Perceptron (MLP) configuration. This form of NN is one of the most popular machine learning methods due to its ability to solve non-linear problems, and helped set the foundations on which modern methods and algorithms lay. Drawing inspiration from biological nervous systems, artificial neural networks emulate synaptic connectivity using computational units called artificial neurons. Each neuron processes input signals through weighted aggregation, followed by non-linear transformation via activation functions to generate outputs [35].

By interconnecting these neurons, or nodes, in layered architectures, diverse network topologies emerge with distinct computational capabilities. The learning process involves iterative optimization of connection weights through backpropagation algorithms, enabling the network to reproduce input-output relationships present in training data.

The MLP model we adopted consists of a feed-forward structure with neurons arranged in sequential layers, trained using the backpropagation method.

3) *Long Short-Term Memory*: As our most advanced model, we selected the LSTM network due to its superior ability to capture temporal patterns in sequential data.

The Long Short-Term Memory networks belong to the family of recurrent neural networks (RNNs), which are specifically designed to retain information across time steps, making them especially effective for sequential data such as time series [34]. LSTMs were introduced by Hochreiter and Schmidhuber [37] as a solution to the vanishing gradient problem that limits the performance of standard RNNs. Their architecture incorporates both long-term and short-term memory units, as well as a set of gating mechanisms (input, forget, and

output gates) that regulate the flow of information. These gates determine when to store, discard, or retrieve information from memory, allowing the model to capture dependencies over sequences [34, 37].

Although the objective of this work is to estimate bottom-hole pressure at the same time step as the input variables, we believe that the use of a sequential architecture can provide greater stability and robustness to the predictions. By capturing temporal dependencies, the model can identify dynamic patterns that might not be apparent in static approaches, resulting in more consistent and reliable predictions.

4) *Transfer Learning*: This relatively recent paradigm in artificial intelligence is based on the idea of using knowledge acquired from one dataset or domain as a foundation or starting point to accelerate and improve training on a different but related problem [38, 39]. This approach is especially useful when working with deep learning models, which typically require large amounts of training data to perform effectively. The framework involves training a machine learning model on a large, often more general dataset, then freezing its parameters (e.g., connection weights) and subsequently adapting the model to a new problem—one that usually lacks sufficient data for traditional deep learning methods, or when data can be easily outdated [38]. The adaptation step in supervised learning problems can be carried out through different approaches, as briefly outlined below [40]:

- **Fine-tuning:** This involves “unfreezing” some or all layers of the base model and retraining it using the new dataset, typically with fewer epochs and/or a smaller learning rate than the initial training phase.
- **Addition of new layers:** In this approach, the base model remains unchanged, and one or more new layers are added. Only the weights of these new layers are adjusted during the additional training.

Both approaches aim to preserve the general features learned by the base model while enabling efficient adaptation to the new problem. Further discussion regarding categories and different approaches to transfer learning can be found in the works of Pan et al. [38] and Weiss et al. [39].

Transfer learning has gained popularity in both scientific and industrial applications, particularly in tasks involving computer vision, natural language processing, and time series modeling [40]. For this latter class of problems, integration with LSTM architecture has also been actively explored in

the literature; application examples range from financial market forecasting [41] to energy demand prediction [42].

In this work, we explore transfer learning for domain adaptation of our BHP estimators, using base models trained on data from a field with a larger number of samples and greater variability. We then test different adaptation strategies for applying these models to a new field with slightly different characteristics. These steps are illustrated in the final blocks of the flowchart in Fig. 3.

### 3.4. Evaluation Metrics

The performance of the estimators was quantitatively evaluated using the metrics Mean Absolute Percentage Error (MAPE), Symmetric Mean Absolute Percentage Error (SMAPE), and Root Mean Squared Error (RMSE), as defined respectively by the equations below:

$$MAPE = \frac{1}{n} \cdot \sum_{j=1}^n \left| \frac{y_j - \hat{y}_j}{y_j} \right| \quad (8)$$

$$SMAPE = \frac{1}{n} \cdot \sum_{j=1}^n \frac{|y_j - \hat{y}_j|}{\frac{(y_j + \hat{y}_j)}{2}} \quad (9)$$

$$RMSE = \sqrt{\frac{1}{n} \cdot \sum_{j=1}^n (y_j - \hat{y}_j)^2} \quad (10)$$

where  $y_j$  are the predicted values and  $\hat{y}_j$  the actual values of the dependent variable [43], in our case, the bottom-hole pressure.

Qualitatively, we will also examine the curves of actual and estimated pressure values over time, assessing the estimators' ability to capture and reproduce trends in pressure behavior, such as during periods of well restrictions, production decline, or response to injection effects.

## 4. Results

We present the results in three phases: in the first we tune hyperparameters for the LSTM and the benchmark NN and ridge regression models using training and validation subsets from our larger oilfield; in the second we evaluate performance for a test subset from the same field, and in the third we evaluate transfer learning for our new oilfield. Both tests simulate real-life situations for oil wells without available PDG data.

Parameter	Values (ranges)
Number of layers	1 to 3
Number of neurons	20 to 300
Dropout	0.05 to 0.50
Loss function	MSE, MAE, SMAPE
Activation function	ReLU, GELU, ELU, Tanh
Learning rate	0.0001 to 0.003

Table 3: **Hyperparameters and their respective ranges evaluated in our neural network models.**

#### 4.1. Hyperparameter Tuning and Model Selection

For hyperparameter tuning and defining the optimal configurations of each selected model, we relied on the training and validation subset extracted from Field 1 data, as illustrated earlier in Fig. 5. This dataset was divided into 5 parts, with wells randomly assigned to each fold, and evaluated using a 5-fold cross-validation scheme. In each step, estimators were trained on four folds and validated on the fifth, as depicted in Fig. 9. Performance metrics were computed using 8, 9, and 10, and final metrics were obtained by averaging results across all folds.

To account for the stochastic nature of ML model training, each configuration was run multiple times, and standard deviations were recorded for subsequent analysis.

This procedure was repeated for every tested model configuration to identify optimized hyperparameter combinations. For the linear regression model, only the regularization coefficient  $\alpha$  was tunable. Neural networks required optimization of network architecture (e.g., layers, nodes), activation functions, loss functions, and learning rate. For LSTM, we added the number of time steps per sample as a tunable parameter. For both NN and LSTM, we evaluated the inclusion of dropout—a regularization technique where randomly selected nodes are temporarily deactivated (weights set to zero before calculating the subsequent layer) during training to mitigate overfitting [34].

Tables 3 and 4 summarize the adjustable parameters and value ranges tested during optimization for the NN and LSTM models, respectively.

Finally, we assessed different input variable combinations, including the full feature set but also testing subsets that excluded variables with possible lower relevance, based on the correlation analysis in Fig. 6 and on our experience. The proposed configurations are displayed in Table 5.

Parameter	Values (ranges)
Number of layers	1 to 3
Number of elements	20 to 200
Dropout	0.05 to 0.50
Error function	MSE, MAE, SMAPE
Activation function	ReLU, Tanh
Timesteps	2 to 15

Table 4: **Hyperparameters and their respective ranges evaluated in our LSTM models.**

Set #	Input variables
Set 1	[Choke P, Choke T, WHP, WHT, $Q_o$ , $Q_g$ , Depth PDG]
Set 2	[Choke P, Choke T, WHP, WHT, $Q_o$ , $Q_g$ , $Q_w$ , Depth PDG]
Set 3	[Choke P, Choke T, WHP, WHT, $Q_o$ , GOR, $W_{cut}$ , Depth PDG]
Set 4	[Choke Ap, Choke P, Choke T, WHP, WHT, $Q_o$ , $Q_g$ , Depth PDG]
Set 5	[Choke P, WHP, $Q_o$ , GOR, $W_{cut}$ , Depth PDG]
Set 6	[Choke P, WHP, $Q_o$ , $Q_g$ , $W_{cut}$ , Depth PDG]

Table 5: **Sets of input variables tested in the model definition.**

To illustrate the results of the search for optimal configurations, Table 6 presents the mean (after multiple runs) of the three error metrics for the top-performing models in our validation set, whose hyperparameters are described below:

- **LR1:** Set 3, *MinMax* scaler,  $\alpha = 0.2$ .
- **NN1:** Set 5, *Standard* scaler, 60 neurons, 0.26 dropout, loss MSE, activation *ReLU*.
- **NN2:** Set 3, *Standard* scaler, 100 neurons, 0.15 dropout, loss MSE, activation *ReLU*.
- **LSTM1:** Set 3, *MinMax* scaler, 2 timesteps, 80 elements, 0.30 dropout, loss MSE, activation *Tanh*.
- **LSTM2:** Set 3, *MinMax* scaler, 3 timesteps, 40 elements, 0.30 dropout, loss MSE, activation *Tanh*.

Model	MAPE	SMAPE	nRMSE
LR1	1.363	1.359	2.047
NN1	1.437	1.432	2.07
NN2	1.466	1.466	2.1
LSTM1	<b>1.349</b>	<b>1.347</b>	<b>1.967</b>
LSTM2	1.398	1.395	2.013
LSTM3	1.501	1.503	2.108

Table 6: **Results obtained with the most representative models for the 5-fold validation.**

- **LSTM3:** Set 3, *MinMax* scaler, 10 timesteps, 40 elements, 0.30 dropout, loss MSE, activation *Tanh*.

Key Observations:

- Performance metrics were very similar across all methods and configurations.
- Linear Regression: Demonstrated minimal sensitivity to the  $\alpha$  parameter, likely due to the dataset characteristics (large sample size, relatively few outliers, and low dimensionality).
- Neural Networks: Models with a single hidden layer outperformed deeper architectures, showing less tendency toward overfitting.
- LSTM: Achieved the best performance, although by a very small margin over the simpler methods. Configurations with a lower number of time steps performed better, in general.
- As for the input variables, Set 3 showed as the best for most configurations, indicating that almost all input variables can add valuable information for the estimation.
- Normalization with *MinMax* scaler was the best option for both LR and LSTM, while NN worked better with *Standard* scaler.

These six top-performing models were selected for further evaluation using the blind test dataset in the next phase.

Model	Test Set 1 (9,410 samples)		
	MAPE	SMAPE	nRMSE
LR1	<b>1.244 <math>\pm 0.0</math></b>	<b>1.256 <math>\pm 0.0</math></b>	<b>1.997 <math>\pm 0.0</math></b>
NN1	1.376 $\pm 0.106$	1.393 $\pm 0.108$	2.174 $\pm 0.094$
NN2	1.341 $\pm 0.160$	1.358 $\pm 0.164$	2.062 $\pm 0.137$
LSTM1	1.309 $\pm 0.071$	1.326 $\pm 0.073$	2.075 $\pm 0.055$
LSTM2	1.452 $\pm 0.233$	1.471 $\pm 0.239$	2.188 $\pm 0.185$
LSTM3	1.468 $\pm 0.106$	1.491 $\pm 0.109$	2.248 $\pm 0.110$

Table 7: Results obtained with the most representative models on the first blind test dataset, for Field 1.

Model	Test Set 2 (7,312 samples)		
	MAPE	SMAPE	nRMSE
LR1	1.355 $\pm 0.0$	1.359 $\pm 0.0$	1.976 $\pm 0.0$
NN1	1.338 $\pm 0.072$	1.337 $\pm 0.076$	1.974 $\pm 0.058$
NN2	1.115 $\pm 0.082$	1.113 $\pm 0.082$	1.770 $\pm 0.095$
LSTM1	1.044 $\pm 0.031$	1.040 $\pm 0.032$	1.695 $\pm 0.025$
LSTM2	1.091 $\pm 0.082$	1.087 $\pm 0.082$	1.726 $\pm 0.071$
LSTM3	<b>1.022 <math>\pm 0.053</math></b>	<b>1.018 <math>\pm 0.054</math></b>	<b>1.626 <math>\pm 0.053</math></b>

Table 8: Results obtained with the most representative models on the second blind test dataset, for Field 1.

#### 4.2. Model Testing for Field 1

For testing our models on Field 1, we utilized the two reserved datasets described earlier (Fig. 5): the first set comprised 09 wells with their complete historical data (excluding the last year), and the second set contained the last year of sensor and production data from all 45 wells in the original dataset.

The results from the optimized models (defined in the previous section), showing mean and standard deviation after multiple runs, are presented in Tables 7 and 8, respectively for those two datasets.

For the best-performing configuration of each estimator type, we plotted the estimated vs. measured value correlations, presenting them in Fig. 10, 11, and 12 for the LR1, NN2, and LSTM1 models, respectively. We included on those references for the error margins, with dashed lines indicating  $\pm 10\%$  and dash-dot lines indicating  $\pm 5\%$  deviations.

As key observations, we highlight stability, minimal outliers, and low error rates, especially compared to most literature benchmarks [29]. More

specifically, we have:

- Good metrics were obtained with the simplest models, with most test samples exhibiting very low errors. This causes the metrics to show little variation when more complex models are introduced.
- Although with very close values, the simplest model, LR, showed the best performance for Test Dataset 1.
- For Test Dataset 2, composed of samples from a wider variety of wells and after a temporal cutoff, the LSTM model showed an advantage by a more significant margin.
- We can observe a slight difference in the dispersion of the estimated samples in relation to the reference line, with an advantage for the LSTM model.

Additionally, we plotted specific examples of temporal analysis for two representative wells, for which we compared measured data with estimates from the top-performing ML models from each of the families (LR, NN, and LSTM). This qualitative approach aligns closely with practical field applications, and is shown in Fig. 13 and 14 for two challenging examples.

The qualitative analysis consistently corroborates the quantitative findings, demonstrating that our top-performing models accurately capture pressure behavior, including transient events like production peaks and operational changes, while maintaining temporal stability. These results are particularly encouraging given the inherent measurement uncertainties present in field data.

One important aspect to be noted is that the LSTM model performs better than the others when we're dealing with extreme conditions, as we can see in our examples. The first (Fig. 13) consists of a well with a long production history and abrupt changes in production behavior due to ICV adjustments, while the second well (Fig. 14) underwent extreme modulation using the choke valve throughout the analyzed period, in addition to experiencing an increasing GOR. Both cases serve as justification for the use of the more complex and computationally demanding method.

The linear regression, however, has the advantage of a training process more repeatable, with no noticeable variance. It can also be easily interpreted by observing the weights attributed to each of the input variables.

Crucially, our findings underscore the fundamental relationship between model performance and training data quality. As we stated in our previous work [30], robustness in the estimates requires datasets that adequately represent the full range of operational scenarios. The current study provides empirical evidence that expanded datasets significantly improve model robustness, yielding more consistent predictions with reduced uncertainty margins. This dataset-size effect proves particularly valuable for machine learning applications where data diversity directly impacts generalization capability.

#### 4.3. Evaluating Transfer Learning for Field 2

In the final phase of our study, we investigated the application of transfer learning strategies for developing soft sensor replacements in scenarios involving new domains (fields or well groups) with insufficient training data for data-intensive supervised learning methods. We evaluated our top-performing LSTM and NN models using the two transfer learning approaches we described in Section III.C: (1) adding a new layer to the original model while keeping pre-trained weights frozen, and (2) fine-tuning the pre-trained model. Both approaches were tested using data from one platform in Field 2 for retraining, with validation performed on two test sets: one containing data from a second platform (excluding the most recent year) and another comprising the final year’s data from both platforms.

Notably, while our Field 1 dataset didn’t include wells operating with gas lift systems, we incorporated this variable for Field 2, allowing better estimates for the wells that use it. This capability to accommodate new input variables is also one of the benefits of the transfer learning framework.

The results presented in Tables 9 and 10 compare error metrics between transfer learning implementations and models trained exclusively on Field 2 data, for both datasets. The metrics demonstrate excellent performance, confirming the methodology’s applicability across different domains.

The fine-tuning approach yielded superior results, with Fig. 15 and 16 showing the estimated *versus* measured value correlations for NN and LSTM models using this technique, compared against baseline cases without transfer learning. It’s clear from the plots that both approaches can benefit from the transfer learning.

Finally, we plotted temporal BHP curves for two representative wells (Fig. 17 and 18), comparing estimates from our best-performing LSTM model with and without the transfer learning against measured pressure data.

Model	Test Set 1 (11,229 samples)		
	MAPE	SMAPE	nRMSE
NN1 <i>w/o TL</i>	7.094 $\pm$ 0.081	6.893 $\pm$ 0.076	7.426 $\pm$ 0.075
NN1 <i>w/ New Layer</i>	2.770 $\pm$ 0.350	2.746 $\pm$ 0.341	3.101 $\pm$ 0.367
NN1 <i>w/ Fine Tuning</i>	2.733 $\pm$ 0.086	2.766 $\pm$ 0.085	3.542 $\pm$ 0.107
LSTM1 <i>w/o TL</i>	3.409 $\pm$ 0.128	3.588 $\pm$ 0.138	5.877 $\pm$ 0.308
LSTM1 <i>w/ New Layer</i>	2.737 $\pm$ 0.346	2.808 $\pm$ 0.376	3.960 $\pm$ 0.620
LSTM1 <i>w/ Fine Tuning</i>	<b>1.564 <math>\pm</math> 0.119</b>	<b>1.574 <math>\pm</math> 0.122</b>	<b>2.042 <math>\pm</math> 0.186</b>

Table 9: Results obtained with representative models on the first test dataset, before and after transfer learning, for Field 2.

Model	Test Set 2 (2,077 samples)		
	MAPE	SMAPE	nRMSE
NN1 <i>w/o TL</i>	5.721 $\pm$ 0.057	5.754 $\pm$ 0.057	6.455 $\pm$ 0.059
NN1 <i>w/ New Layer</i>	1.581 $\pm$ 0.250	1.574 $\pm$ 0.245	1.941 $\pm$ 0.288
NN1 <i>w/ Fine Tuning</i>	1.143 $\pm$ 0.053	1.144 $\pm$ 0.053	1.435 $\pm$ 0.052
LSTM1 <i>w/o TL</i>	1.000 $\pm$ 0.153	1.006 $\pm$ 0.156	1.209 $\pm$ 0.177
LSTM1 <i>w/ New Layer</i>	1.178 $\pm$ 0.136	1.169 $\pm$ 0.133	1.660 $\pm$ 0.154
LSTM1 <i>w/ Fine Tuning</i>	<b>0.809 <math>\pm</math> 0.146</b>	<b>0.808 <math>\pm</math> 0.145</b>	<b>1.041 <math>\pm</math> 0.200</b>

Table 10: Results obtained with representative models on the second test dataset, before and after transfer learning, for Field 2.

In Fig. 17, we bring a well with a long production history, which underwent significant changes such as major depletion and increases in GOR and water cut. The estimation remains highly accurate throughout the entire history. In the example shown in Fig. 18, we have a recently drilled well with a history of high flow rates and significant restrictions in its opening. Also in this case, the BHP estimation maintained an error below 2% throughout the analyzed history. These results further validate both the quality of our methodology and its applicability to diverse operational scenarios.

Regarding computational efficiency, LSTM models required substantially longer training times (1-2 minutes per configuration) when running on a multi-processor cluster, compared to MLP neural networks (0.4 s) and regression models (0.075 s). However, all trained models achieved inference times of just milliseconds. This performance enables wells without an available PDG to be seamlessly integrated with PI systems for continuous data tracking and analysis, making them fully suitable for real-time monitoring applications such as reservoir management, artificial lift optimization, inflow performance analysis, and early detection of well anomalies.

## 5. Conclusions

This work presented a practical application of machine learning in the oil and gas industry, deploying deep learning in the form of Long Short-Term Memory and transfer learning techniques to obtain estimators for the bottom-hole pressure in oil wells.

Our approach is purely data-driven, using as input variables the pressures and temperatures measured at the wellheads and on the platform, as well as the fluid production rates. To estimate the BHP, we used as a flagship model the LSTM, and as benchmarks MLP neural networks and regularized (ridge) linear regression.

We evaluated our framework in real-world scenarios, using data from a group of offshore platforms operating in the Brazilian pre-salt basin. First, we applied it to wells producing from a single giant oilfield, from which we obtained small errors, with  $MAPE < 1.5\%$  in our blind tests for a broad range of production conditions under regular flow. Although simpler models are already capable of delivering good results in most situations, the model with temporal dependency proved to be more efficient in more unusual situations and in future use simulations, which justifies its application despite its greater complexity and computational cost.

Subsequently, we evaluated transfer learning strategies, using the model trained on the first dataset as a base model for a second oilfield that had a smaller and less diverse history, also including a new variable—the gas lift rate required for some wells. We observed that the approach of fine-tuning using new data was the most effective and produced errors of the same order of magnitude as our first case.

With that, we demonstrated the applicability of the proposed methodology to diverse practical situations in oil and gas production, including important features such as adaptability to new domains and robustness to concept drift. The idea of a soft sensor for bottom-hole measurements can therefore be useful for offline studies or real-time monitoring (given the availability of wellhead and topside sensor data). Such estimators can be used as backup or reference in digital twin systems or effectively replacing physical gauges in situations where they fail or when their installation is technically or economically prohibitive. The data-driven estimators can thus be considered valuable alternatives to ensure the availability of essential data for production monitoring and reservoir management, aiming at safe and efficient operations, together with value maximization.

## References

- [1] A. C. Gringarten, T. v. Schroeter, T. Rolfsvaag, J. Bruner, Use of down-hole permanent pressure gauge data to diagnose production problems in a north sea horizontal well, in: SPE Annual Technical Conference and Exhibition?, SPE, 2003, pp. SPE-84470.
- [2] E. A. Antonelo, E. Camponogara, B. Foss, Echo state networks for data-driven downhole pressure estimation in gas-lift oil wells, *Neural Networks* 85 (2017) 106–117.
- [3] R. E. V. Vargas, C. J. Munaro, P. M. Ciarelli, A. G. Medeiros, B. G. do Amaral, D. C. Barrionuevo, J. C. D. de Araújo, J. L. Ribeiro, L. P. Magalhães, A realistic and public dataset with rare undesirable real events in oil wells, *Journal of Petroleum Science and Engineering* 181 (2019) 106223.
- [4] P. H. Paulo, F. C. Pereira, H. V. Ayala, System identification techniques for soft sensors and multiphase flow metering, *IFAC-PapersOnLine* 58 (15) (2024) 538–543.

- [5] S. Van Gisbergen, A. Vandeweijer, Reliability analysis of permanent downhole monitoring systems, *SPE Drilling & Completion* 16 (01) (2001) 60–63.
- [6] H. Zheng, B. Lin, J. Jiang, Y. Jin, L. Peng, Knowledge-guided machine learning method for downhole gauge record prediction in deep water gas field, in: Offshore Technology Conference Asia, OTC, 2024, p. D031S020R004.
- [7] F. Curreri, L. Patanè, M. G. Xibilia, Soft sensor transferability: A survey, *Applied Sciences* 11 (16) (2021) 7710.
- [8] T. Ahmed, Chapter 6 - fundamentals of reservoir fluid flow, in: T. Ahmed (Ed.), *Reservoir Engineering Handbook* (Fourth Edition), fourth edition Edition, Gulf Professional Publishing, Boston, 2010, pp. 331–483. doi:<https://doi.org/10.1016/B978-1-85617-803-7.50014-6>.
- [9] P. A. Mal’Tsev, A. S. Natal’Ya, S. E. Abramkin, M. E. Podkina, Designing a digital twin in oil and gas technologies: Technology integration, in: 2024 XXVII International Conference on Soft Computing and Measurements (SCM), IEEE, 2024, pp. 352–355.
- [10] A. Satter, G. M. Iqbal, 4 - reservoir fluid properties, in: A. Satter, G. M. Iqbal (Eds.), *Reservoir Engineering*, Gulf Professional Publishing, Boston, 2016, pp. 81–105. doi:<https://doi.org/10.1016/B978-0-12-800219-3.00004-8>.
- [11] W. Ruan, C. Zhou, H. Yang, Z. Wang, B. Sun, Y. Bai, A review on the recent process of lazy wave risers, *Journal of Marine Science and Engineering* 12 (11) (2024) 2000.
- [12] H. Fang, M. Duan, Chapter 3 - marine petroleum (gas) engineering and equipment, in: H. Fang, M. Duan (Eds.), *Offshore Operation Facilities*, Gulf Professional Publishing, Boston, 2014, pp. 341–536. doi:<https://doi.org/10.1016/B978-0-12-396977-4.00003-2>.
- [13] G. Yadigaroglu, G. Hetsroni, G. F. Hewitt, Flow regimes, in: G. Yadigaroglu, G. F. Hewitt (Eds.), *Introduction to Multiphase Flow: Basic Concepts, Applications and Modelling*, Springer International Publishing, Cham, 2018, pp. 95–140. doi:[https://doi.org/10.1007/978-3-319-58718-9\\_4](https://doi.org/10.1007/978-3-319-58718-9_4).

- [14] D. H. Beggs, J. P. Brill, A study of two-phase flow in inclined pipes, *Journal of Petroleum technology* 25 (05) (1973) 607–617.
- [15] H. Duns Jr, N. Ros, Vertical flow of gas and liquid mixtures in wells, in: *World Petroleum Congress, WPC, 1963*, pp. WPC–10132.
- [16] A. R. Hagedorn, K. E. Brown, Experimental study of pressure gradients occurring during continuous two-phase flow in small-diameter vertical conduits, *Journal of Petroleum technology* 17 (04) (1965) 475–484.
- [17] L. O. Seman, L. K. Miyatake, E. Camponogara, C. M. Giuliani, B. F. Vieira, Derivative-free parameter tuning for a well multiphase flow simulator, *Journal of Petroleum Science and Engineering* 192 (2020) 107288. doi:<https://doi.org/10.1016/j.petrol.2020.107288>.
- [18] H. Zalavadia, V. Sabharwal, S. Sankaran, Continuous bottomhole pressure estimation using machine learning and physics-based methods—a field case study, in: *International Petroleum Technology Conference, IPTC, 2024*, p. D031S099R003.
- [19] C. A. Akinseye, O. O. Omotara, A. Giwa, Determination of flowing bottom-hole pressure of a well using modified guo's model, *Journal of Environmental Science, Computer Science and Engineering & Technology* 9 (2) (2020) 270–286.
- [20] X. Li, J. Miskimins, B. T. Hoffman, A combined bottom-hole pressure calculation procedure using multiphase correlations and artificial neural network models, in: *SPE Annual Technical Conference and Exhibition?*, SPE, 2014, pp. SPE–170683.
- [21] L. A. Aguirre, B. O. Teixeira, B. H. Barbosa, A. F. Teixeira, M. C. Campos, E. M. Mendes, Development of soft sensors for permanent downhole gauges in deepwater oil wells, *Control Engineering Practice* 65 (2017) 83–99.
- [22] D. Campos, D. D. K. Wayo, R. B. De Santis, D. A. Martyushev, Z. M. Yaseen, U. I. Duru, C. M. Saporetti, L. Goliatt, Evolutionary automated radial basis function neural network for multi-phase flowing bottom-hole pressure prediction, *Fuel* 377 (2024) 132666. doi:<https://doi.org/10.1016/j.fuel.2024.132666>.

- [23] C. C. Nwanwe, U. I. Duru, An adaptive neuro-fuzzy inference system white-box model for real-time multiphase flowing bottom-hole pressure prediction in wellbores, *Petroleum* 9 (4) (2023) 629–646. doi:<https://doi.org/10.1016/j.petlm.2023.03.003>.
- [24] D. Opoku, A. Al-Ghamdi, A. Osei, Novel method to estimate bottom hole pressure in multiphase flow using quasi-monte carlo method, in: International Petroleum Technology Conference, IPTC, 2020, p. D021S050R001.
- [25] M. Firouzi, S. Rathnayake, Prediction of the flowing bottom-hole pressure using advanced data analytics, in: Asia Pacific Unconventional Resources Technology Conference, Brisbane, Australia, 18-19 November 2019, Unconventional Resources Technology Conference, 2020, pp. 735–742.
- [26] F. H. Al Shehri, A. Gryzlov, T. Al Tayyar, M. Arsalan, Utilizing machine learning methods to estimate flowing bottom-hole pressure in unconventional gas condensate tight sand fractured wells in saudi arabia, in: SPE Russian Petroleum Technology Conference, SPE, 2020, p. D043S032R002.
- [27] O. Olamigoke, D. C. Onyeali, Machine learning prediction of bottomhole flowing pressure as a time series in the volve field, *International Journal of Frontiers in Engineering and Technology Research* 2 (2) (2022) 020–039.
- [28] S. Sanusi, A. Omisore, E. Blankson, C. Anyanwu, O. Eremiokhale, Estimation of bottom hole pressure in electrical submersible pump wells using machine learning technique, in: SPE Nigeria Annual International Conference and Exhibition, SPE, 2021, p. D021S009R003.
- [29] O. E. Agwu, S. Alatefi, A. Alkouh, R. R. Suppiah, Modelling the flowing bottom hole pressure of oil and gas wells using multivariate adaptive regression splines, *Journal of Petroleum Exploration and Production Technology* 15 (2) (2025) 22.
- [30] M. A. Fernandes, E. Gildin, M. A. Sampaio, Data-driven estimation of flowing bottom-hole pressure in petroleum wells using long short-term memory, in: 2024 International Conference on Machine

Learning and Applications (ICMLA), IEEE, 2024, pp. 1530–1537. doi:10.1109/ICMLA61862.2024.00236.

- [31] J. Brownlee, Machine learning mastery with Python: understand your data, create accurate models, and work projects end-to-end, Machine Learning Mastery, Australia, 2021.
- [32] M. M. Mukaka, A guide to appropriate use of correlation coefficient in medical research, *Malawi medical journal* 24 (3) (2012) 69–71.
- [33] V. G. Raju, K. P. Lakshmi, V. M. Jain, A. Kalidindi, V. Padma, Study the influence of normalization/transformation process on the accuracy of supervised classification, in: 2020 Third International Conference on Smart Systems and Inventive Technology (ICSSIT), IEEE, 2020, pp. 729–735.
- [34] A. Zhang, Z. Lipton, M. Li, A. Smola, *Dive Into Deep Learning*, Cambridge University Press, 2023.
- [35] S. J. Russell, P. Norvig, *Artificial intelligence: a modern approach* (4th edition), Pearson, Upper Saddle River, NJ, 2021.
- [36] J. K. Kalita, D. K. Bhattacharyya, S. Roy, *Fundamentals of Data Science*, Academic Press, 2024. doi:<https://doi.org/10.1016/B978-0-323-39177-8.00012-0>.
- [37] S. Hochreiter, J. Schmidhuber, Long short-term memory, *Neural computation* 9 (8) (1997) 1735–1780.
- [38] W. Pan, E. Xiang, N. Liu, Q. Yang, Transfer learning in collaborative filtering for sparsity reduction, in: *Proceedings of the AAAI conference on artificial intelligence*, Vol. 24, 2010, pp. 230–235.
- [39] K. Weiss, T. M. Khoshgoftaar, D. Wang, A survey of transfer learning, *Journal of Big data* 3 (2016) 1–40.
- [40] M. Iman, H. R. Arabnia, K. Rasheed, A review of deep transfer learning and recent advancements, *Technologies* 11 (2) (2023) 40.
- [41] M. Tahir, S. Ali, A. Sohail, Y. Zhang, X. Jin, Unlocking online insights: Lstm exploration and transfer learning prospects, *Annals of Data Science* 11 (4) (2024) 1421–1434.

- [42] D. Kim, Y. Lee, K. Chin, P. J. Mago, H. Cho, J. Zhang, Implementation of a long short-term memory transfer learning (lstm-tl)-based data-driven model for building energy demand forecasting, *Sustainability* 15 (3) (2023) 2340.
- [43] B. E. Flores, A pragmatic view of accuracy measurement in forecasting, *Omega* 14 (2) (1986) 93–98. doi:[https://doi.org/10.1016/0305-0483\(86\)90013-7](https://doi.org/10.1016/0305-0483(86)90013-7).

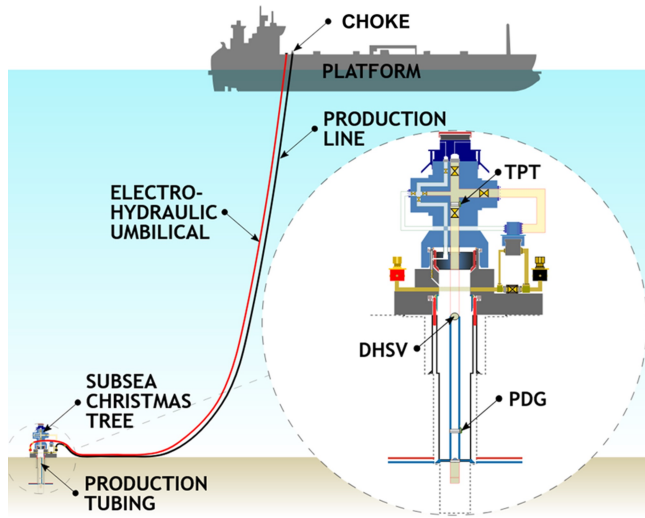


Figure 1: Schematic of an offshore production system, highlighting the positioning of the most relevant equipment and sensors (reproduced from [3]).

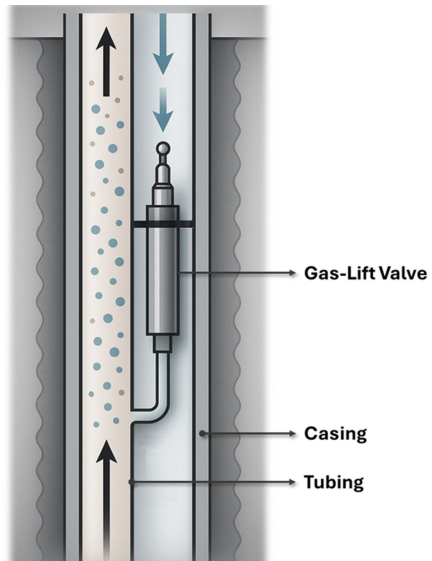


Figure 2: Schematic representation of a gas lift valve operating within an oil well. *Note: image enhanced using ChatGPT.*

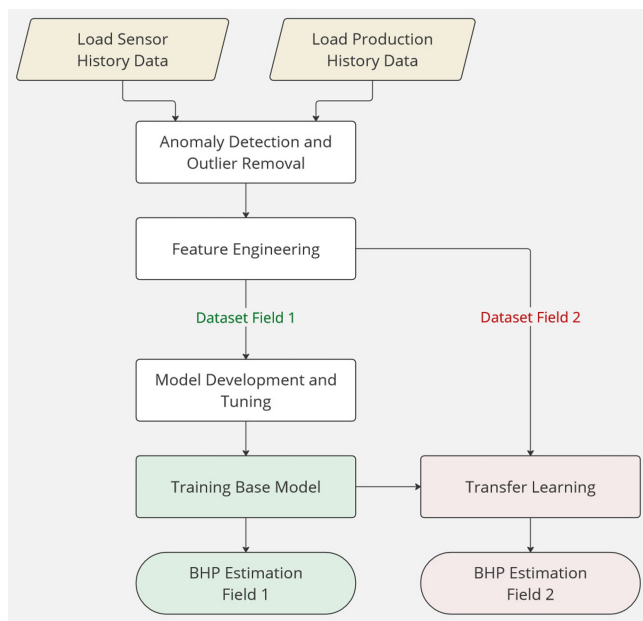


Figure 3: Flowchart depicting the proposed methodology, including base model training and transfer learning.

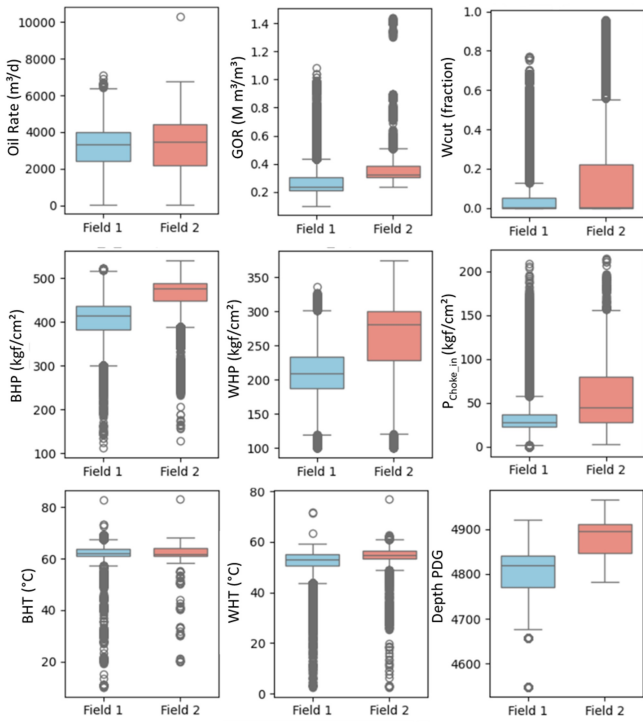


Figure 4: Boxplots showing the probability distributions of the variables for the two fields.

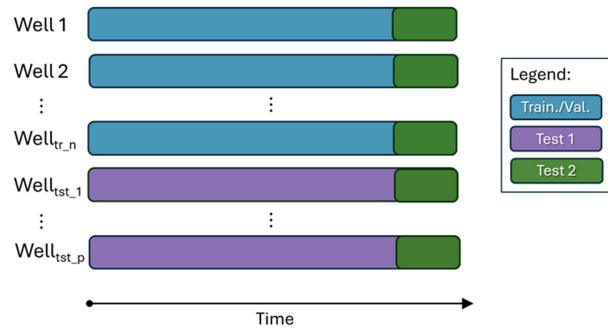


Figure 5: Dataset partitioning.

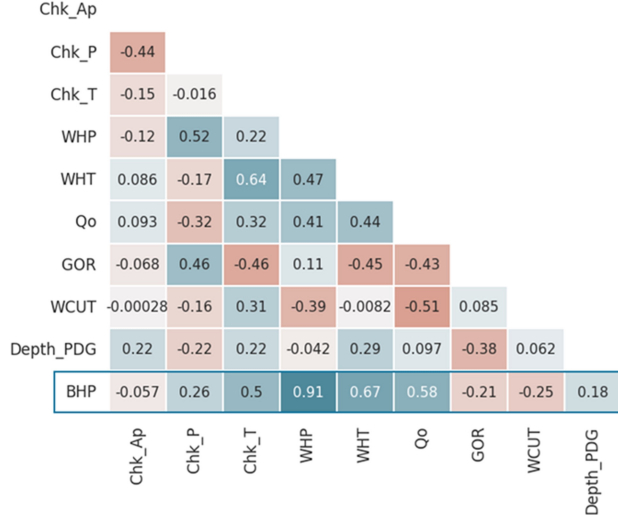


Figure 6: Correlation heatmap for the variables of the problem.

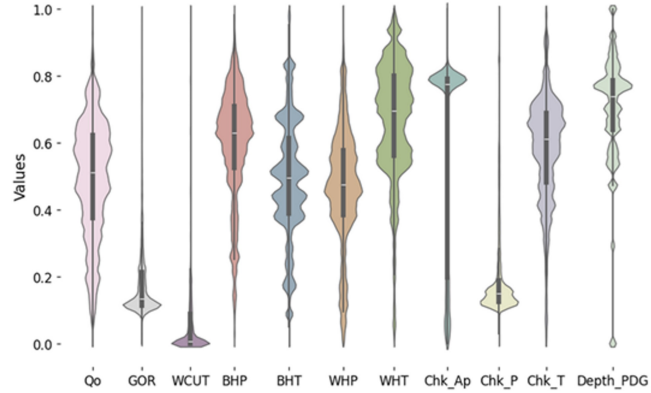


Figure 7: Violin plots of the variables after *MinMax* normalization for Field 1.

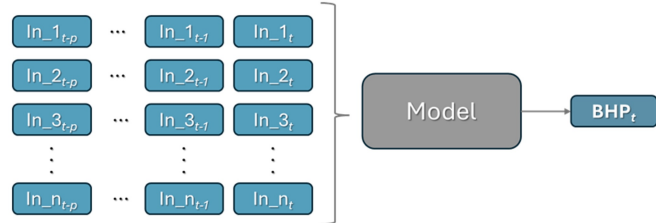


Figure 8: Input samples preparation.

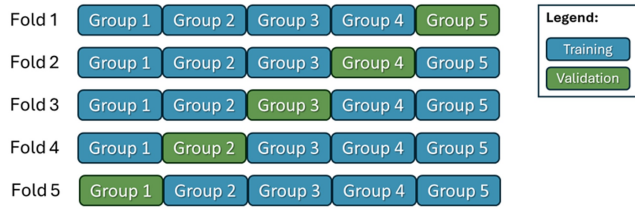


Figure 9: Dataset preparation for training and 5-fold cross-validation.

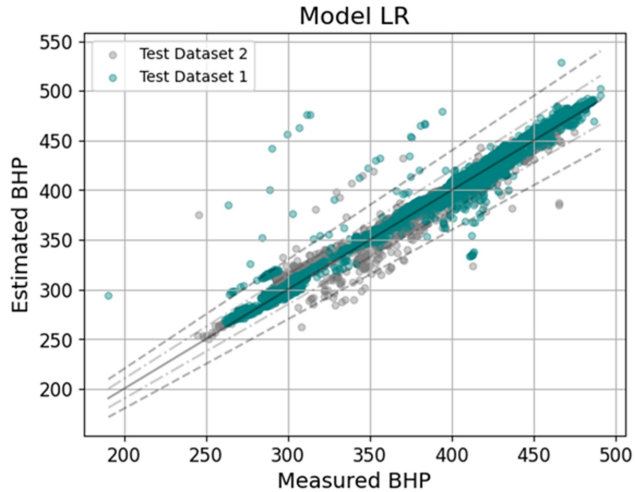


Figure 10: Correlation of estimated versus actual values for the BHP from our best linear regression model (Field 1).

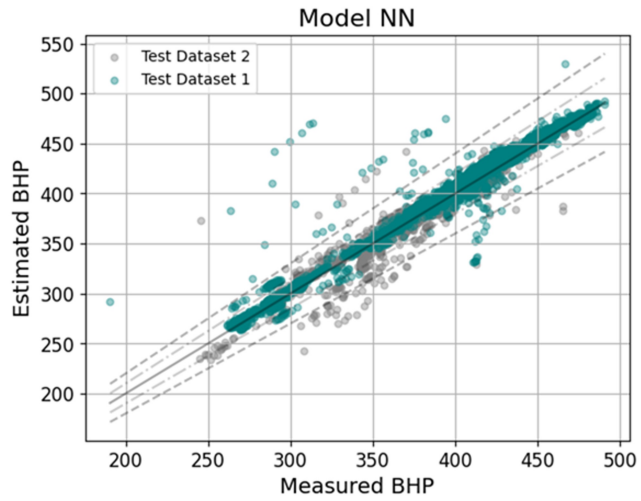


Figure 11: Correlation of estimated versus actual values for the BHP from our best neural network model (Field 1).

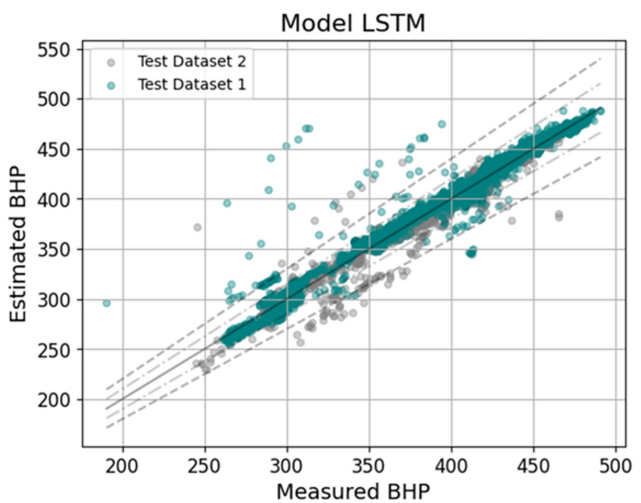


Figure 12: Correlation of estimated versus actual values for the BHP from our best LSTM model (Field 1).

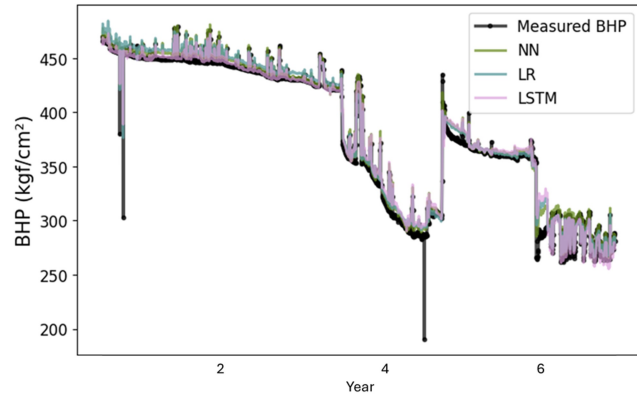


Figure 13: BHP estimates with the three selected models, applied to a well with long production history and abrupt changes in production behavior due to ICV adjustments (Field 1).

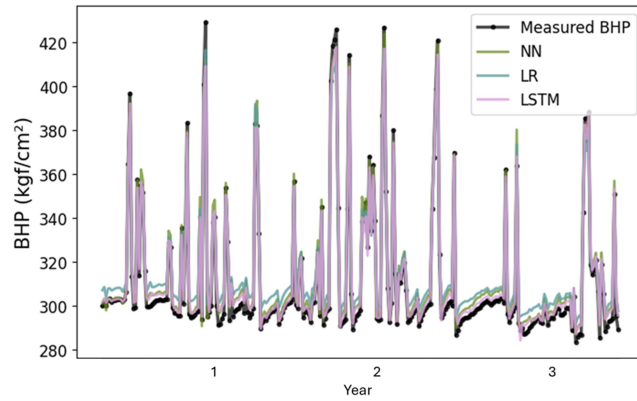


Figure 14: BHP estimates with the three selected models, applied to a well that experienced a significant increase in GOR over time and numerous production control adjustments (Field 1).

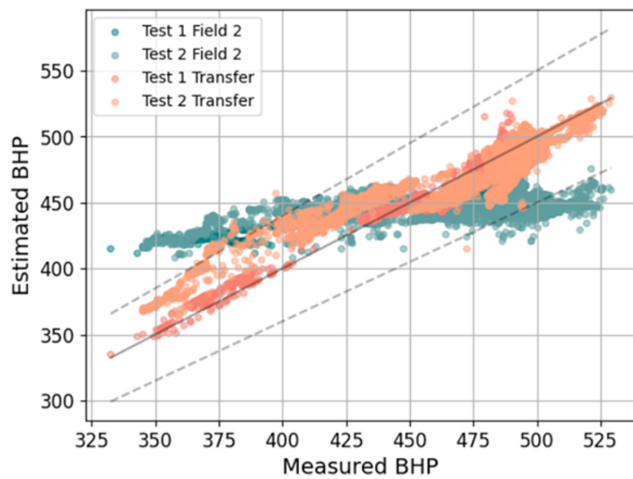


Figure 15: Correlation of estimated versus actual values for the BHP from our best NN model before and after transfer learning (Field 2).

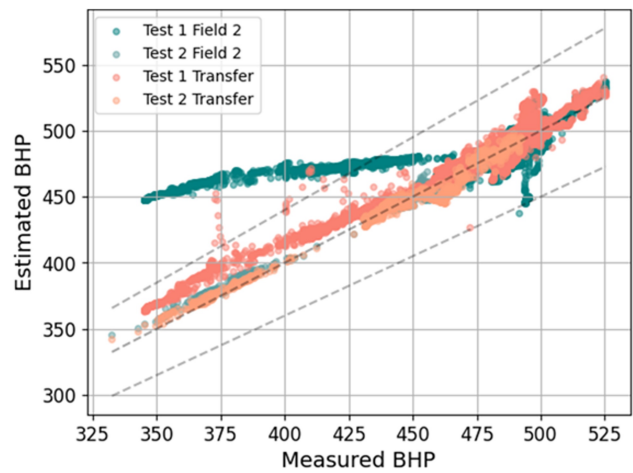


Figure 16: Correlation of estimated versus actual values for the BHP from our best LSTM model before and after transfer learning (Field 2).

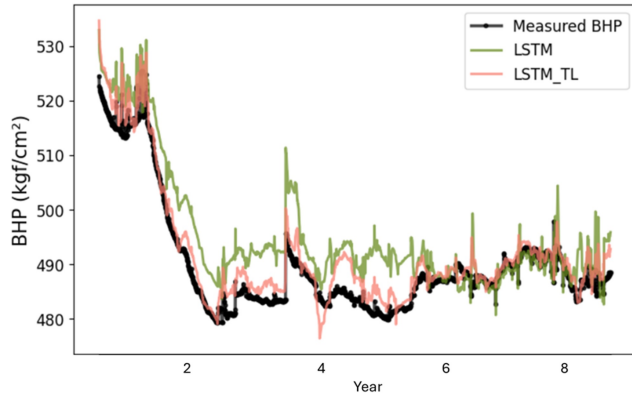


Figure 17: BHP estimates with the selected models, applied to a well with long production history (Field 2).

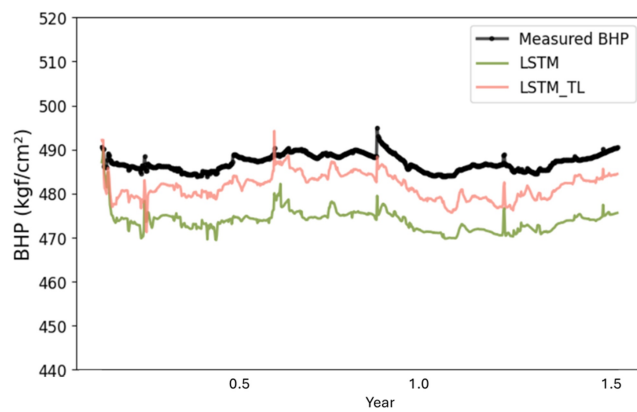


Figure 18: BHP estimates with the selected models, applied to a recently drilled well (Field 2).